Controlling Morphology in Polycrystalline Films by Nucleation and Growth from Metastable Nanocrystals

Ajay Singh[1,2], Lukas Lutz[2 //], Gary K Ong[1,3 //], Karen Bustillo[2], Simone Raoux[4], Jean L. Jordan-Sweet[5], Delia J. Milliron[1,2*]

[1]McKetta Department of Chemical Engineering, The University of Texas at Austin, Austin, Texas 78712, USA
[2] National Center for Electron Microscopy, Molecular Foundry, Lawrence Berkeley National Laboratory, Berkeley, California 94720, USA
[3] Department of Materials Science and Engineering, University of California—Berkeley, Berkeley, California 94720, USA
[4] Helmholtz-Zentrum Berlin für Materialien und Energie GmbH, Albert-Einstein-Str. 15, 12489 Berlin, Germany.
[5] IBM Watson Research Center, 1101 Kitchawan Road, Yorktown Heights, New York 10598, United States
[//] These authors contributed equally to this work.
***Corresponding authors. E-mail:** milliron@che.utexas.edu*

Supporting Information

Materials. Copper (II) acetylacetonate ($Cu(acac)_2$, 99.99%), Tin(IV) acetate ($Sn(OAc)_4$, >99.99%), Zinc acetate ($Zn(OAc)_2$, >99.99%), 1-dodecanethiol (1-DDT, >97%), tert-dodecanethiol (t-DDT, 98.5%, mixture of isomers), Trioctylphosphine oxide (TOPO, 99%) and 1-octadecene (ODE, 90%, technical grade), Formamide (≥99.5%), 2,6-difluoropyridine (99%), were purchased from Aldrich. Germanium diselenide ($GeSe_2$) powder was purchased from Alfa Aesar. Ultrapure hydrazine was purchased from Arch Chemicals. All chemicals were used as received without any further purification.

Synthesis of CZTS nanocrystals (Nanorod and spherical). CZTS nanocrystals were synthesized following the previous published method with a small modification.[1] In a typical synthesis, $Cu(acac)_2$ (1.332 mmol), Zinc $(OAc)_2$ (0.915 mmol), Tin $(OAc)_4$ (0.75 mmol), TOPO (4 mmol) and 10 ml of 1-octadecene were loaded in a three-neck round-bottom flask and degassed at room temperature for 15-30 mins. The reaction mixture was further heated in an inert atmosphere with continuous stirring to 250°C. When the temperature reached 155°C, a mixture of 0.5 mL1-DDT and 3.5mL t-DDT (*in the case of nanorods*) was injected into the flask which resulted in an immediate color change from dark green to light yellow and then finally to brown *[in the case of spherical nanocrystals, only 1-DDT (4 ml) was used]*. After injection, the reaction was allowed to proceed for 15-30 minutes with continuous stirring. The nanocrystal growth was quenched by injecting 2- 3 mL of anhydrous toluene in the reaction flask at 80°C. After that the nanocrystals

were washed with 1:1 ratio of toluene and ethanol and centrifuged at 4000 rpm for 5 minutes in a glove box. The resultant nanocrystals were re-dispersed in toluene and stored in a glove box for further use.

Chalcogenidometallate Cluster (ChaMs) synthesis: ChaMs were prepared in an inert atmosphere in a nitrogen glovebox by simply dissolving the $GeSe_2$ in anhydrous hydrazine in the presence of excess Se at room temperature. 5.0 mmol of $GeSe_2$ and 5.0 mmol of Se were added to 5.0 mL of anhydrous hydrazine in a 40 ml vial and left under continuous stirring for a week. During that time, the solution color changed from black to optically clear yellow. The solution was then filtered through a 0.2 μm filter to remove any undissolved solids and then dried under nitrogen flow to obtain a yellow powder with the chemical formula $(N_2H_5)_4Ge_2Se_6$. These clusters were then used for the ligand exchange through a phase transfer protocol. For typical ligand exchange, the ChaM clusters were dissolved in formamide at a concentration of approximately 15 - 20 mg mL^{-1}. After ligand exchange, nanocrystals were dispersed in either formamide or 2,6-difluoropyridine using gentle sonication.

Caution! Hydrazine is highly toxic and should be handled with extreme caution to prevent exposure by inhalation or absorption through the skin.

Nanocrystal Film Formation: Pristine nanocrystals (in toluene) and ChaM-coated nanocrystals (in 2,6-difluoropyridine) were cast onto silicon substrates (a razor blade was used to smooth the surface) and dried slowly (15-20 min) under solvent saturated conditions to form crack free thin films. Nanocrystal composite thin films with varying ChaM concentration (adjusted after ligand exchange, to make high and low loading nanocrystal composites) were also prepared using the same deposition technique.

Electron Microscopy: The CZTS nanocrystals were characterized by transmission electron microscopy (TEM), annular dark-field scanning transmission electron microscopy with either a JEOL JEM-2011F or a FEI TitanX 80-300 both operating at an accelerating voltage of 200 kV. Cross-sectional images and EDAX analysis of thin film were acquired using Zeiss Gemini Ultra-55 Analytical Scanning Electron Microscope. Prior to imaging, the films were cryofractured after immersion in liquid N2 to provide a clean surface.

In-situ **X-ray Diffraction:** Time-resolved XRD measurements were performed during rapid thermal annealing in a purified He atmosphere at beamline X20C of the National Synchrotron

Light Source at Brookhaven National Laboratory. Various heating rates, from 0.1 to 9 K s^{-1}, were used to anneal the nanocrystals (spherical and nanorod) and their composites with ChaMs. A boron nitride heater stage was used in the chamber that anneals and the intensity of the XRD peaks was detected by a fast linear diode array detector that monitors the intensity of the XRD peaks over a 2θ range of 15°. The centre of the detector was located at 2θ = 31.5°, which allowed the detection of the main strong peaks for both wurtzite (100, 002 and 101) and kesterite (112). The x-ray wavelength was 1.797 Å. To determine the transition temperatures, the diffracted intensity of (100), (002)/(112) and (101) peaks was integrated over an angular range of 1°, and the inflection point of this integrated intensity curve was used to identify the transition temperature as shown in Figure S3.

Ex-situ annealing experiments: Films of the nanocrystals (spherical and nanorod) and their composite films were annealed under an inert atmosphere using rapid thermal annealing. (Ulvac Thermal Annealer).

X-ray Diffraction Analysis: The samples for X-ray diffractogram (XRD) analysis were prepared by drop-casting the nanocrystal dispersion on a silicon substrate. The analysis was carried out on a Bruker AXS D8 Discover GADDS X-Ray Diffractometer using Cu Kα radiation, 1.54 Å, with a HighStar area detector. To analyze the grain size, we used the high intensity peak of the kesterite phase (2θ = 28.5˚for Cu= 1.54Å) to do a gaussian peak fit to obtain the peak width (FWHM). The Scherrer equation ($d = K\lambda / b\cos\theta$, where factor K = 0.89, λ =0.154 nm for Cu Kα radiation, d is crystallite size, b is the peak width) was used to calculate the average grain size of the sample. Note: The overall peak width was deconvolute from the instrumental broadening [using this expression, $b = (B^2 - \beta^2)^{1/2}$, where B is the peak width of kesterite phase (2θ = 28.5˚) and β is instrumental peak broadening] before applying the Scherrer equation. For example, the XRD patterns for the kesterite (112) peak from thin films obtained by annealing the CZTS nanocrystals (spheres) resulted in an estimated grain size for the nanosphere films of approximately ~ 95 nm. These grain sizes are matched well with the estimated from SEM analysis (100 ± 20, an average of 100 grains).

Raman Spectroscopy: Raman measurements of annealed thin films were carried out at room temperature on a Horiba Jobin Yvon LabRAM ARAMIS system. A green laser (wavelength = 532 nm) was used for excitation.

Differential Scanning Calorimeter (DSC) measurement: A Q200 DSC (TA Instruments) was used to determine the heat released during phase transition from wurtzite to kesterite for nanocrystal (nanorod and spherical) and the composite with ChaMs, scanning from 100 to 400 °C (spherical), 450 °C (nanorod), and 550 °C (CZTS-GeSe) at a heating rate of 10 °C/min. To prepare the samples, several milligrams of nanocrystals or nanocomposite in were drop-cast into an alumina crucibles, and the solvent was allowed to evaporate.

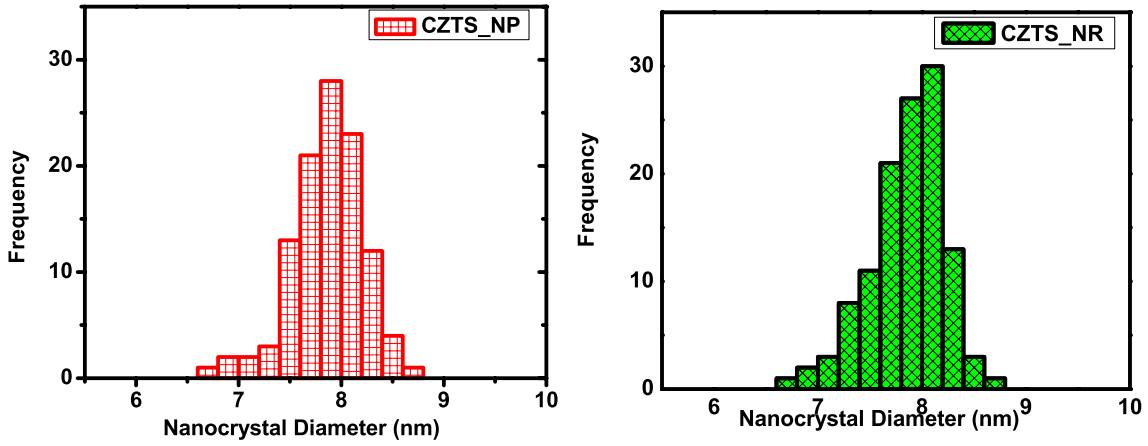

Figure S1: CZTS nanoparticle (sphere) and nanorod diameter distribution histograms before annealing in thin films.

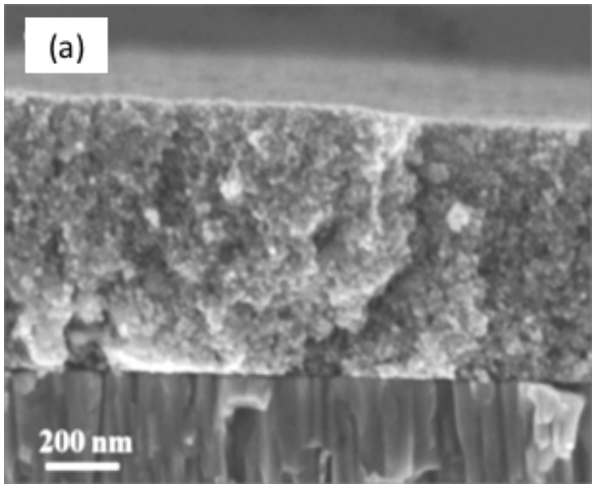

Figure S2: Cross-sectional SEM images shows thin film with small grains obtained from kesterite CZTS nanocrystals.

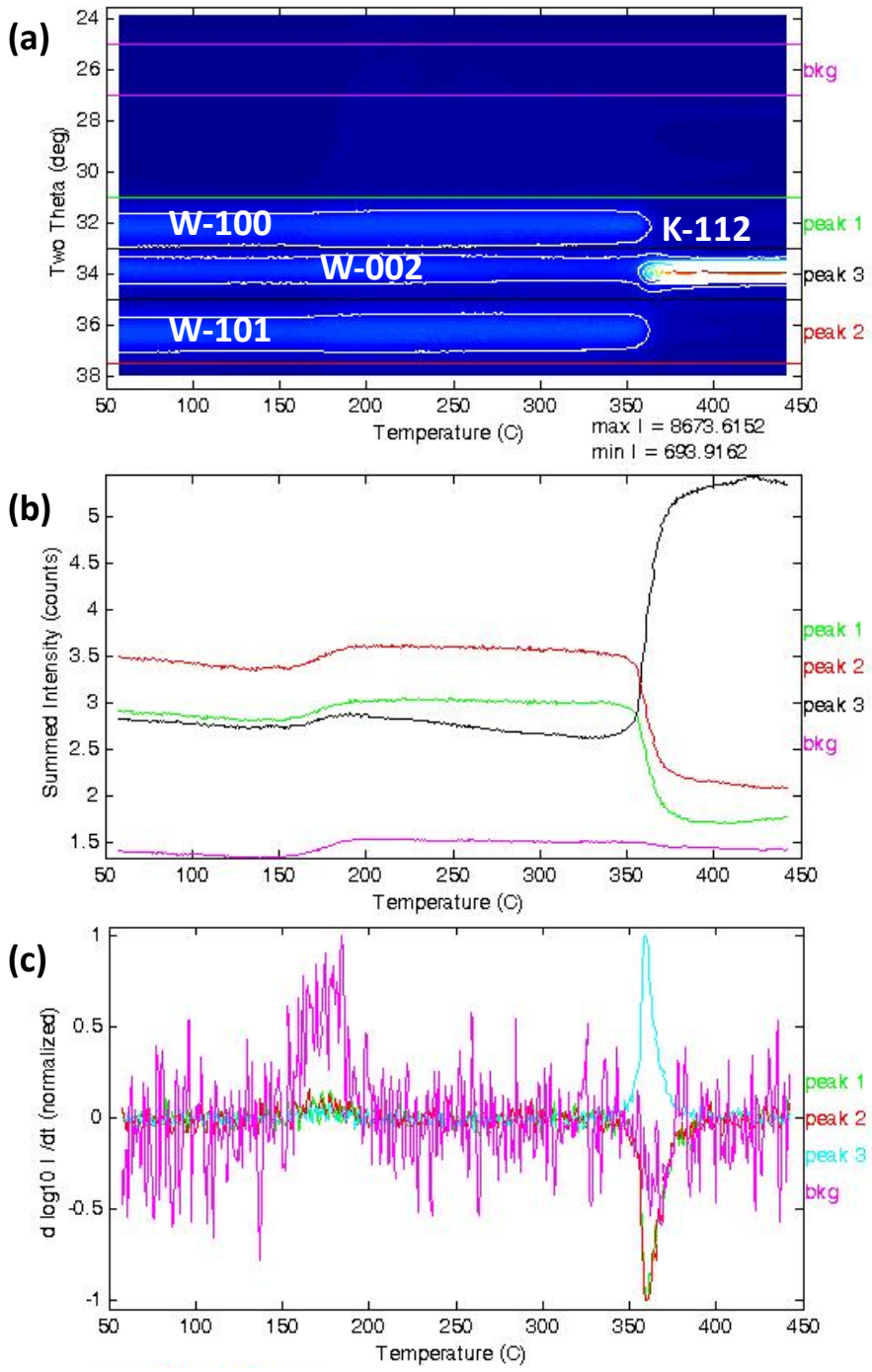

Figure S3: The phase-transition temperature (*e.g. for spheres*) was determined by integrating the diffracted intensity for (100), (002)/(112) and (101) peaks (a) over an angular range of 1°, and the inflection point of this integrated intensity curve was used to identify the transition temperature (b & c).

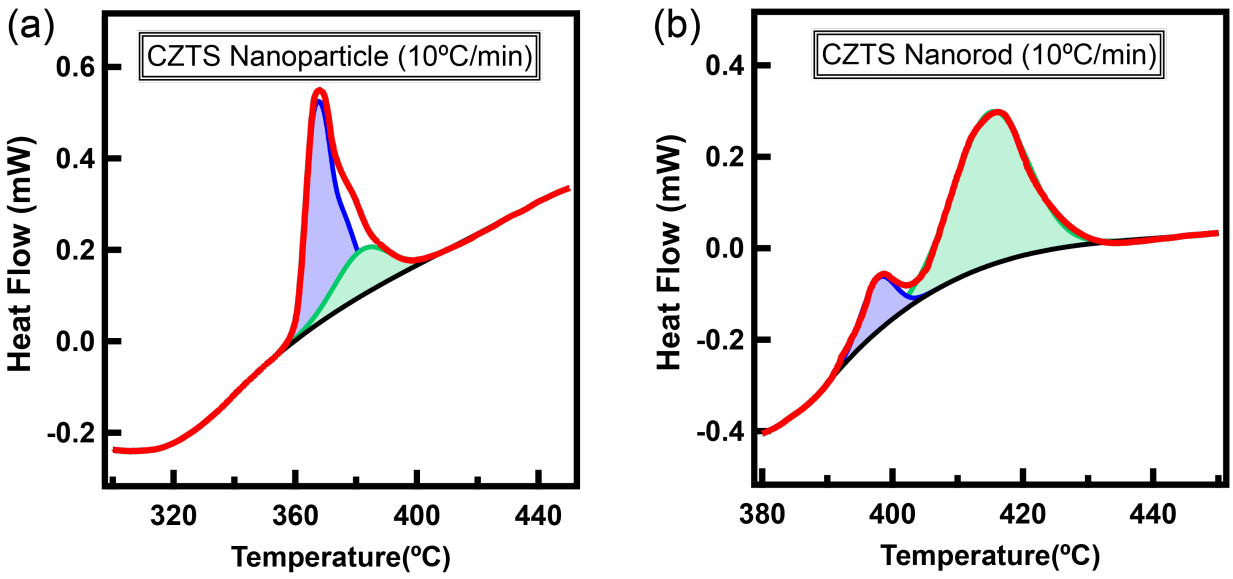

Figure S4: DSC graphs for the CZTS **(a)** spherical and **(b)** nanorod films show the two peak behaviour corresponding to nucleation and growth of the kesterite phase thin film.

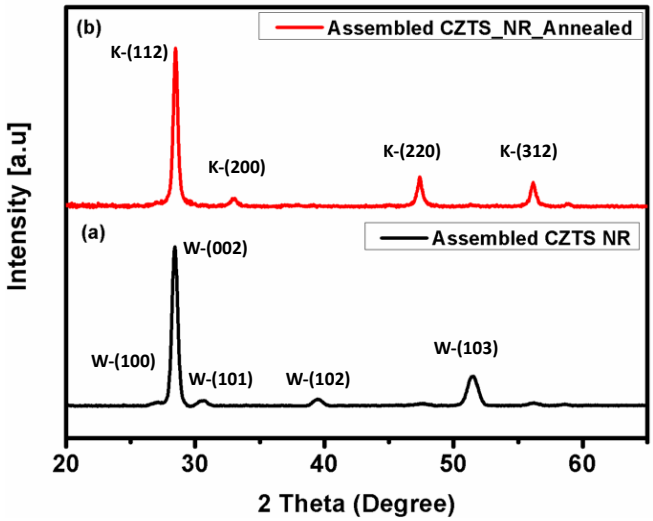

Figure S5: XRD patterns of an assembled CZTS nanorod sheet before (a) and after annealing (b). The difference between the K(112) at 29.8 (2 theta) degrees and the W(002) at 29.9 (2 theta) degrees is within the resolving power of the instrument.

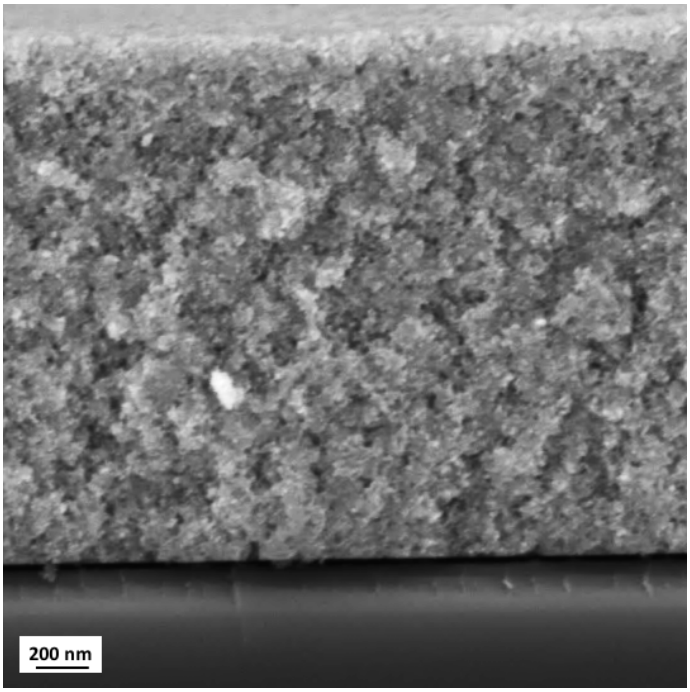

Figure S6: Cross-sectional SEM image of a CZTS nanosphere composite thin film obtained after annealing for 15 min at 550 °C under N_2 atmosphere.

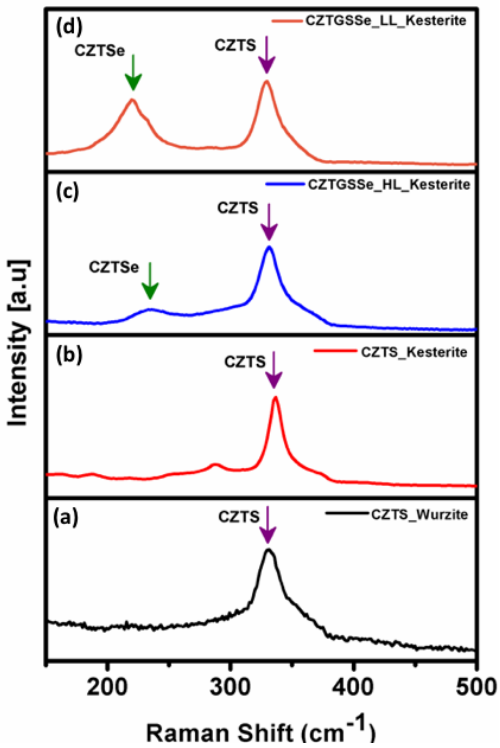

Figure S7: Raman spectra of as-synthesised wurtzite nanorods (a) and after phase transformation to kesterite (b) show the main "A" mode for these structures. (c) & (d) Raman spectra of annealed

nanocomposite thin films obtained from high (c) and low (d) loading of nanocrystals in the Ge-Se matrix shows both the A modes for the CZTS and CZTSe. This emergence and the shift (with increasing amount of Se) of the A mode for CZTSe is matched well with the literature. [2,4]

References:

1. Singh, A.; Geaney, H.; Laffir, F.; Ryan, K. M. *J. Am. Chem. Soc.* **2012** *134*, 2910–2913.
2. Khadka, D. B.; Kim, S. Y.; Kim, J. H. *J. Phys. Chem. C* **2016**, *120*, 4251–4258.
3. Singh, A.; Singh, S.; Levcenko, S.; Unold, T.; Laffir, F.; Ryan, K. M. *Angew. Chem., Int. Ed*. **2013**, *52*, 9120–9124.
4. Khare, A.; Himmetoglu, B.; Cococcioni, M.; Aydil, E. S. *J. Appl. Phys.* **2012**, *111*, 123704.